Since January 2020 Elsevier has created a COVID-19 resource centre with free information in English and Mandarin on the novel coronavirus COVID-19. The COVID-19 resource centre is hosted on Elsevier Connect, the company's public news and information website.

Chemical Engineering Journal 418 (2021) 129392

Contents lists available at ScienceDirect

Chemical Engineering Journal

journal homepage: www.elsevier.com/locate/cej

Inhalable nanovaccine with biomimetic coronavirus structure to trigger mucosal immunity of respiratory tract against COVID-19

Bin Zheng [a,1,*], Wenchang Peng [a,1], Mingming Guo [a], Mengqian Huang [b], Yuxuan Gu [a], Tao Wang [b], Guangjian Ni [a], Dong Ming [a,*]

[a] Academy of Medical Engineering and Translational Medicine, Tianjin Key Laboratory of Brain Science and Neural Engineering, Tianjin University, 92 Weijin Road, Nankai District, Tianjin 300072, PR China

[b] School of Life Sciences, Tianjin University, 92 Weijin Road, Nankai District, Tianjin 300072, PR China

ARTICLE INFO

Keywords:
SARS-CoV-2
COVID-19
Bionic coronavirus structure
Inhalable nanovaccine
Respiratory mucosal immunity

ABSTRACT

The COVID-19 pandemic caused by SARS-CoV-2 seriously threatens global public health. It has previously been confirmed that SARS-CoV-2 is mainly transmitted between people through "respiratory droplets". Therefore, the respiratory tract mucosa is the first barrier to prevent virus invasion. It is very important to stimulate mucosal immunity to protect the body from respiratory virus infection. Inspired by this, we designed a bionic-virus nanovaccine, which can induce mucosal immunity by nasal delivery to prevent virus infection from respiratory tract. The nanovaccine that mimic virosome is composed of poly(I:C) mimicking viral genetic material as immune adjuvant, biomimetic pulmonary surfactant (bio-PS) liposomes as capsid structure of virus and the receptor binding domains (RBDs) of SARS-CoV-2 as "spike" to completely simulate the structure of the coronavirus. The nanovaccine can be administered by inhaling to imitate the process of SARS-CoV-2 infection through the respiratory tract. Our results demonstrated that the inhalable nanovaccine with bionic virus-like structure has a stronger mucosal protective effect than routine muscle and subcutaneous inoculation. In particular, high titer of secretory immunoglobulin A (sIgA) was detected in respiratory secretions, which effectively neutralize the virus and prevent it from entering the body through the respiratory tract. Through imitating the structure and route of infection, this inhalable nanovaccine strategy might inspire a new approach to the precaution of respiratory viruses.

1. Introduction

Severe acute respiratory syndrome coronavirus-2 (SARS-CoV-2) quickly spread around the world and caused serious social panic because of its high infectivity and higher fatality rate than ordinary influenza viruses.[1,2] Corona Virus Disease 2019 (COVID-19) has been listed as a pandemic by the WHO, resulted the developments of the effective vaccine play a crucial role.[3–5] At present, several attempts have been made to the research and development of the COVID-19 vaccines, including inactivated vaccines, live attenuated vaccines, recombinant protein vaccines, vectored vaccines, DNA vaccines and RNA vaccines.[6–11] Most of these vaccines are already in pre-clinical studies, and some have even begun to be widely administered in the population. [12] FDA (Food and Drug Administration) have issued emergency use authorization for first COVID-19 vaccine, including Pfizer-BioNTech and Moderna vaccines.[13,14] Although these vaccines play an important role in preventing infection and transmission of the SARS-CoV-2, there are still some weaknesses.[15] For example, DNA vaccines based on viral vectors have the risk of integrating viral oncogenes into a subject's genome and causing normal cell cancerization.[16] Although the safety of mRNA vaccine has been well guaranteed, whether the virus antigen expressed *in vivo* has the correct spatial structure and post-translational modification cannot be controlled.[17] If mRNA cannot guide the synthesis of viral structural proteins with the correct three-dimensional structure and group modification *in vivo*, it is difficult for mRNA vaccine to activate effective protection against the SARS-CoV-2.[18] In addition, due to the fragility of mRNA molecules, it is necessary to modify the two ends of mRNA molecules, and maintain the extremely strict cold chain distribution and cryopreservation.[19] For recombinant protein vaccines represented by the receptor binding domain (RBD)

* Corresponding authors.
E-mail addresses: binzheng@tju.edu.cn (B. Zheng), richardming@tju.edu.cn (D. Ming).
[1] These authors contributed equally to this work.

https://doi.org/10.1016/j.cej.2021.129392
Received 11 January 2021; Received in revised form 22 February 2021; Accepted 12 March 2021
Available online 19 March 2021

antigen of SARS-CoV-2, it is hard to effectively induce the immune response due to its relatively low molecular weight and simple structure. Moreover, it is worth mentioning that almost all of these vaccines are immunized by intramuscular, while the SARS-CoV-2 virus is transmitted through the respiratory tract, so it is difficult to effectively induce the mucosal immunity of the antiviral through these administration methods.[20]

The transmission method of SARS-CoV-2 is similar to that of influenza virus, which mainly infects the body through the respiratory tract.[21] Therefore, the respiratory tract mucosa is the first line of defense to prevent respiratory virus from invading the human body.[22] In view of the unique infection and transmission mode of respiratory virus, which is different from hepatitis virus, HIV and rabies virus, the excitation of respiratory mucosal immunity is one of the most important ways to protect the body from virus infection.[21] Consider these characteristic, the recent rise of nasal delivery flu vaccine is expected to become a new therapeutic tool with great potential.[23–25] After mucosal immunization induced by nasal delivery vaccine, the secretion of respiratory mucosa contains a large amount of secretory immunoglobulin A (sIgA), which can effectively neutralize the invading virus and make it unable to bind to the receptor cells.[26,27] Compared with nasal delivery, intramuscular and subcutaneous injections are difficult to induce highly efficient mucosal immunity in subjects because the antigen does not pass through the respiratory mucosa. In addition, nasal delivery immunity can avoid pain and greatly reduce the risk of potential infection, which is easy for the subjects to accept. The Centers for Disease Control and Prevention (CDC) reported that some nasal delivery vaccines can achieve the same titer of antibody in the blood as injectable vaccines, and approved the clinical use of nasal delivery influenza vaccine.[28,29] Inspired by these, we envisioned the method of nasal delivery to be used in COVID-19 vaccine.

So far, researchers have synthesized nanoparticles with different structures and biological functions, including polymer particles,[30–32] micelles,[33,34] liposomes,[35] nanogels[36,37] and mesoporous material[38,39] for drug delivery. These nanoplatforms can help regulate immunostimulatory or immunosuppression by delivering and releasing antigens, adjuvants and immunomodulators. To stir up mucosal immunity in the respiratory tract, we designed a SARS-CoV-2 like virosome platform containing capsid, nucleic acid and spike protein. Here, we used a biomimetic pulmonary surfactant (bio-PS) layer mimetic "capsid" composed of DPPC/DPPG/DPPE-COOH/Chol.[40,41] And the outer layer of PS covalently linked RBD as the "spike protein" to form a virosome, which mimicked the structure of SARS-CoV-2, and played the role of aggregation and combination of RBD antigen, thus enhanced the immunogenicity of RBD.[42] Poly(I:C) is a synthetic double-stranded RNA, which can be used as the core genetic material of the virosome and induce innate immunity by stimulating Toll-like receptor 3 (TLR3) pathway.[43] This inhalable nanovaccine can get into alveolar macrophages (AMs) and alveolar epithelial cells (AECs) with the help of surfactant proteins A (SP-A) and D (SP-D) without damaging the pulmonary

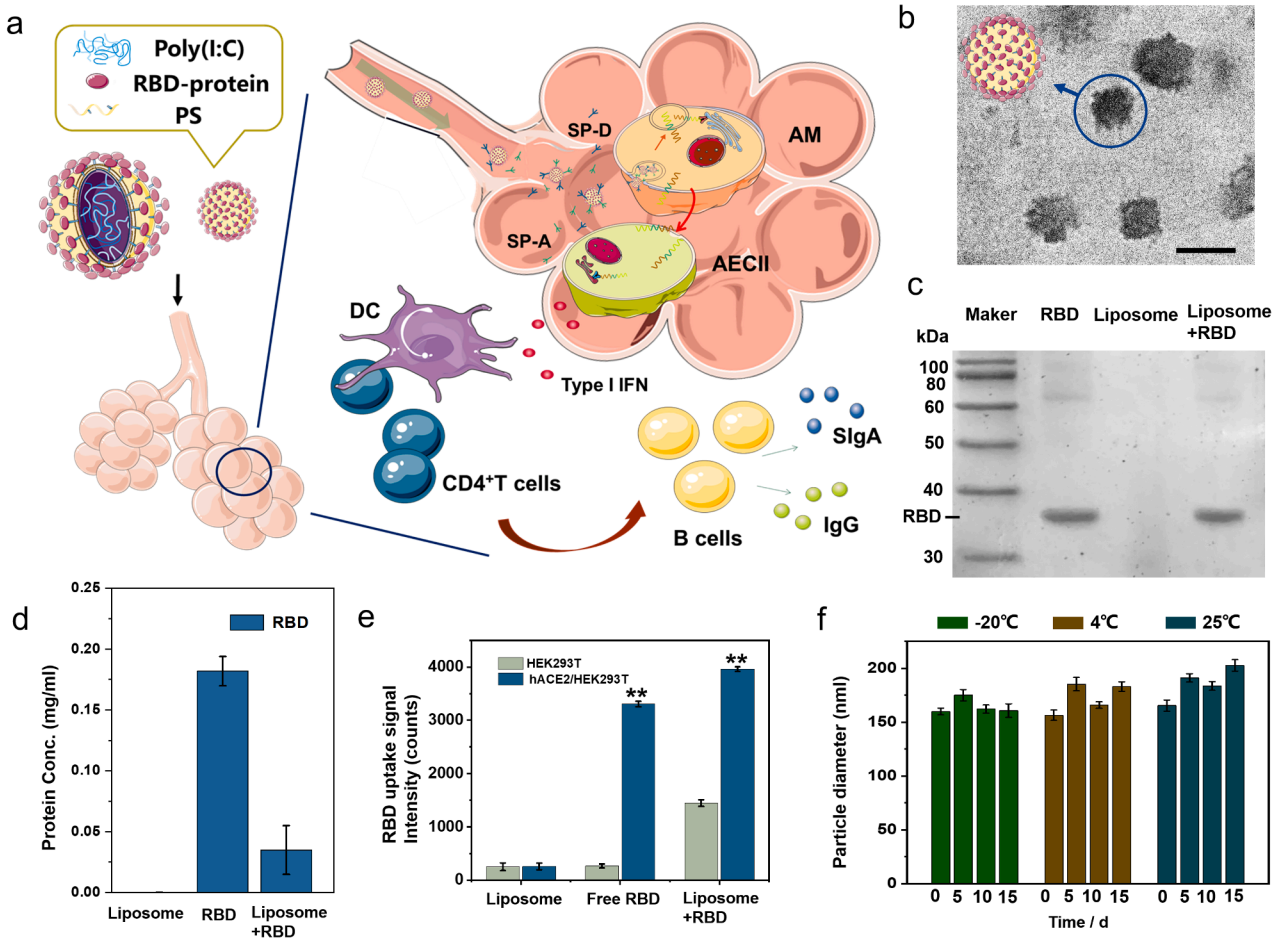

Fig. 1. (a) Schematic diagram of inhalable bionic-virus nanovaccine activating cellular immunity and humoral immunity of respiratory mucosa. (b) TEM images of bionic-virus particles. Scale bars, 200 nm. (c) Coomassie blue staining results of RBD protein. (d) The concentration of protein in the supernatant of the solution is detected by nanodrop. (e) The fluorophore-labeled RBD in free or particulate form binds to HEK-293T cells expressing hACE2. (f) The stability of bionic-virus particles in PBS at different temperatures, pH = 7.0, 0.2 mg/mL, PDI = 12–18%. (For interpretation of the references to colour in this figure legend, the reader is referred to the web version of this article.)

surfactant to induce mucosal immunity (Fig. 1a).[44] In the process of mucosal immune excitation, the extracellular segment of polyclonal immunoglobulin receptor (pIgR) in epithelial cells combine with polyclonal immunoglobulin A (IgA) produced by effector B cells to form sIgA in the mucosal surface, which neutralize viruses in the respiratory tract to prevent them from adhering to and invading recipient cells.[45] Intramuscular injection is the main route of administration for vaccines currently developed, but nasal delivery may be an attractive and more efficacious route.[46] The inhalable nanovaccine mimic the structure and invasion mode of SARS-CoV-2 as much as possible, and better induce the mucosal immunity of the inoculator. The importance and originality of this study are that it explores inhalable immunizations induce mucosal immunity more efficiently than injectable methods to neutralize SARS-CoV-2, which this inhalable nanovaccine strategy might inspire a new approach to the precaution of respiratory viruses.

2. Experimental section

2.1. Reagents and materials.

Bionic PS layer liposome material including 1,2-dipalmitoyl-*sn*-glycero −3-phosphocholine (DPPC), dipalmitoyl phosphatidylglycerole (DPPG), cholesterol, (2,3-Dioleoyloxy-propyl)-trimethylammonium (DOTAP) and 1,2-dipalmitoyl-*sn*-glycero-3-phosphoethanolamine-N-[methoxy(polyethyleneglycol)-1000]–COOH (DPPE-PEG1000-COOH) were bought from Sigma-Aldrich. Immune agonist Poly(I:C) was purchased from MedChemExpress. TNF-α, IL-6 and IFN- β (mouse) ELISA Kit and Commassie Blue Staining Kit were bought from AmyJet Scientific. SARS-CoV-2 (2019-nCoV) Spike pseudovirus and receptor binding domain (RBD) antigen were bought from Genomeditech (Shanghai) Co., Ltd.

2.2. Synthesis of bionic-virus nanovaccine.

Dissolve 13 mg DPPC, 2 mg DPPG, 2 mg DPPE-PEG-COOH, 1 mg cholesterol in 1 ml chloroform, dissolve poly(I:C) in 300 μl enzyme-free sterile water, sonicate under vacuum for 30 min, vacuum and evaporate to remove water molecules. Then, 1 ml PBS was added for hydration, and then sonicated for 15 min to obtain a bionic PS layer liposome (NN). Replace DPPG with DOTAP in the PN component, the specific synthesis process is the same as above. Add EDC (10 mg/ml) /NHS (10 mg/ml) to the bionic PS layer liposome solution, react for 15 min, add RBD protein (RBD: liposome = 2:1), stir at room temperature for 1 h to obtain bionic-virus nanovaccine.

2.3. Characterization of bionic-virus nanovaccine.

The particle size and zeta potential of bionic-virus nanovaccine was measured in a laser scatterometer (Zetasizer Nano ZS90. Malvern). The TEM experiment was performed in a JEOL electron microscope (JEM100CXII). The protein concentration in the solution is measured by Thermo NanoDrope 2000. RB release curve is measured by fluorescence spectrophotometer (RF-6000). The functional verification of the assembled RBD is by co-cultivating the assembled or unassembled RBD particles or free RBD with HEK-293T cells expressing hACE2 for 4 h, then washing them with PBS three times to measure the fluorescence content in the cells. All RBD proteins are labeled with GFP.

2.4. Mouse specific antibody detection and neutralization test of pseudovirus.

Antibody detection adopts indirect ELISA method. In short, RBD protein (1 μg/ml) was coated on the well plate and stored overnight at 4 ℃. The serum and lung lavage fluid of each group were diluted and added into the pre-coated well plate for incubation at 37 ℃ for 30 min. Next, the enzyme labeled anti antibody was added and incubated for 30 min. Add TMB color liquid to incubate in the dark for 15 minutes. Finally, the stop solution was added, and the absorbance was measured the absorbance at 450 nm with a microplate reader. In the pseudovirus neutralization test, mouse serum or BALF was diluted in different multiples, incubated with GFP labeled pseudovirus for 30 min, and then added to hACE2/HEK-293T cells. After 48 h of co-cultivation, the intracellular fluorescence content was measured to verify the protective effect of the serum or BALF against pseudovirus.

2.5. Animal experiment.

To evaluate the *in vivo* immune stimulation of the vaccine, C57BL/6 female mice (5–6 weeks, SPF level) were purchased from Huafukang, China. Cationic liposome DOTAP was used as a transfection reagent to encapsulate the hACE2 plasmid, which was dripped from the nasal cavity to transfect the mouse respiratory tract to construct an hACE2 mice model. All experiments related to the pseudovirus were completed in the P2 laboratory. All the animal experiments involved in this work were approved by the Animal Ethics Committee of Tianjin University.

3. Results and discussion

3.1. Generation and characterization of inhalable bionic-virus nanovaccine.

The pulmonary surfactant layer (PS) is a mixture of lipid and protein secreted by type II alveolar epithelial cells (AEC II), which forms a strong barrier to separate the external air from the alveolar epithelium and prevent nanoparticles and hydrophilic molecules from entering alveolar epithelial cells (AECs). Therefore, the delivery of nanovaccine to AECs remains a substantial challenge. We used the biomimetic pulmonary surfactant (bio-PS) layer composed of DPPC/DPPG/DPPE-COOH/Chol as the delivery carrier with the help of surfactant proteins A (SP-A) and D (SP-D), the bio-PS layer liposomes can enter into AECs without damaging the pulmonary surfactant to induce mucosal immunity. Inspired by the structure of SARS-CoV-2, the virosome formed by bio-PS layer liposomes encapsulating poly (I:C) were prepared by reverse-phase evaporation, and had a particle size of about 110 nm (Figure S1). RBD that binds to host susceptible cells is regarded as promising antigens for many recombinant-protein-based COVID-19 vaccine candidates.[47,48] RBD could be connected with DPPC-COOH in the liposome under the catalysis of EDC/NHS, thereby connecting to the liposome surface to form the spike protein of the bionic virion. The hydrodynamic diameter of the assembled bionic-virus liposome is about 154 nm, which is close to the size of a real virus (Figure S1). As shown in Fig. 1b, bionic-virus particles had a spike structure similar to SARS-CoV-2. RBD band was found in the assembled biomimetic liposomes, which proved that RBD protein was successfully assembled on the liposomes (Fig. 1c). In order to verify the assembly efficiency of RBD protein, we detected the protein concentration of liposome supernatant, initial RBD protein solution, and the supernatant of the solution after the assembly of RBD protein and liposome (Fig. 1d). After calculation, the RBD protein loading rate was about 84%. In addition, the amide bond formed by EDC/NHS reaction was checked by fourier transform infrared spectrometer (FTIR), which proved that the connection between protein and particles was stable (Figure S2). Subsequently, in order to confirm that the assembled RBD still binds to angiotensin-converting enzyme 2 (ACE2), the receptor of SARS-CoV-2, the RBD assembled/unassembled liposomes or free RBD were co-cultured with hACE2/HEK-293T cells, which expressing human ACE2 (hACE2) protein. As shown in Fig. 1e, the RBD uptake of RBD liposome group was the highest, which indicated that the assembled RBD still had complete structure and could bind to hACE2. Due to the granulation caused by assembly, the binding effect of RBD was stronger.

We next investigated the stability and release efficiency of bionic-virus particles. Under the condition of pH = 7.0, the bionic-virus particles had no significant change in particle size at different temperatures,

and maintained good stability within 15 days (Fig. 1f). Bionic-virus particles also had excellent stability in different buffers (pH = 7.0) (Figure S3). The surface of the bionic virus particles was negatively charged and remained stable for two weeks (Figure S4). In addition, we measured the second virial coefficient A_2 of the bionic-virus particles solution (Figure S5). The value of A_2 was greater than zero, indicating that intermolecular repulsion is dominant and macromolecular aggregation will not occur. These results indicated that the bionic-virus particles were stable in solution. However, bionic-virus particles were unstable under acidic conditions (pH = 5.0), and liposomes increase in particle size (Figure S6). Subsequently, we studied the release of liposomes under simulated lysosome environmental conditions. Water soluble rhodamine B (RB) was encapsulated in liposomes and its release was examined in PBS with pH = 5.0 by recording intensity changes of the fluorescence absorption intensity in the supernatant of the solution (Figure S7). As time increased the released amount of RB also increases, and the released amount reaches the maximum at 5 h.

The negatively charged liposome was closest to the pulmonary surfactant (PS) layer in lipid composition and charge.[41] We synthesized positive liposome as a control group to study the absorption of the two liposomes by the macrophages. The main difference between the two was that the liposome surface carries the opposite potential (Figure S8), therefor, we called the two liposomes negative liposome (NL) and positive liposome (PL). Except that the negative DPPG in the liposome component was replaced by the positive DOTAP, the other components of NL and PL were identical. As Figure S9 shown that the internalization of NL in RAW 246.7 was less than that of positively charged PL, which might be explained by the lack of surfactant proteins A and D under *in vitro* culture conditions. Therefore, next we purified PS from BALF and incubated it with the liposomes for 45 min before adding them to RAW 264.7. After treatment, the endocytosis of NL is significantly increased, while the endocytosis of PL has little change. It can be concluded that NL needs to rely on surfactant protein A and D to enter macrophages. Flow cytometry was used to detect the amount of rhodamine fluorescence absorbed by mouse alveolar macrophages (AM) after nasal delivery for 5 h (Figure S10). The results of *in vivo*

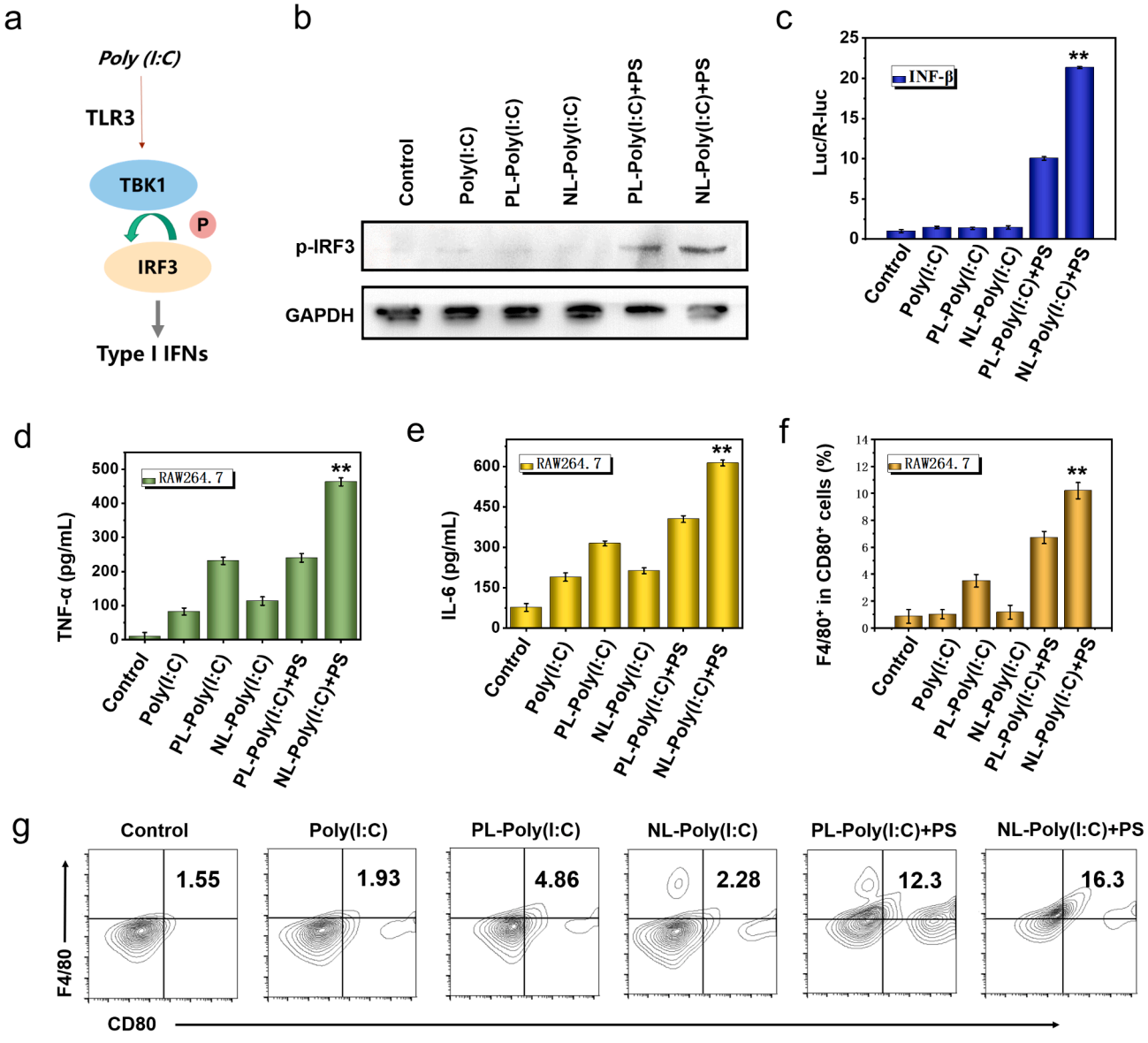

Fig. 2. Verification of immune excitation performance of bionic-virus nanovaccine *in vitro*. (a) Schematic diagram of TLR3 signaling pathway activation. (b) Western blot results of phosphorylated IRF-3 protein. (c) The activation of INF-β in HEK-293 T cells through dual-luciferase reporter assay system. (d, e) Secretion levels of TNF-α (d) and IL-6 (e) in RAW 246.7 cells. (f) Statistic analysis of $CD80^+$ $F4/80^+$ cells in RAW 246.7 cells after 24 h of different treatments. (g) Representative flow cytometric analysis of $CD80^+$ and $F4/80^+$ of (f).

experiments were also consistent with cell experiments. Next, we co-cultured the bionic-virus particles with dendritic cells (DCs) for 24 h. Figure S11 showed that the bionic-virus nanovaccine has good cell compatibility without causing cell death. The MTT experiment also got the same result (Figure S12). In DCs and macrophages, the toxicity of the bionic-virus nanovaccine was very small, and there was no damage to the cells.

3.2. *Verification of immune activation performance of inhalable bionic-virus nanovaccine in Vitro.*

Interferon is a cytokine protein that can activate human immune cells, effectively interfere with virus replication, and enhance the host's defenses.[49–51] Toll-like receptor 3 (TLR3) signaling pathway plays a very important role in the antiviral immune response.[52] The activation of TLR3 signaling pathway can induce the production of IFN-β, which can trigger a further antiviral response by binding to the

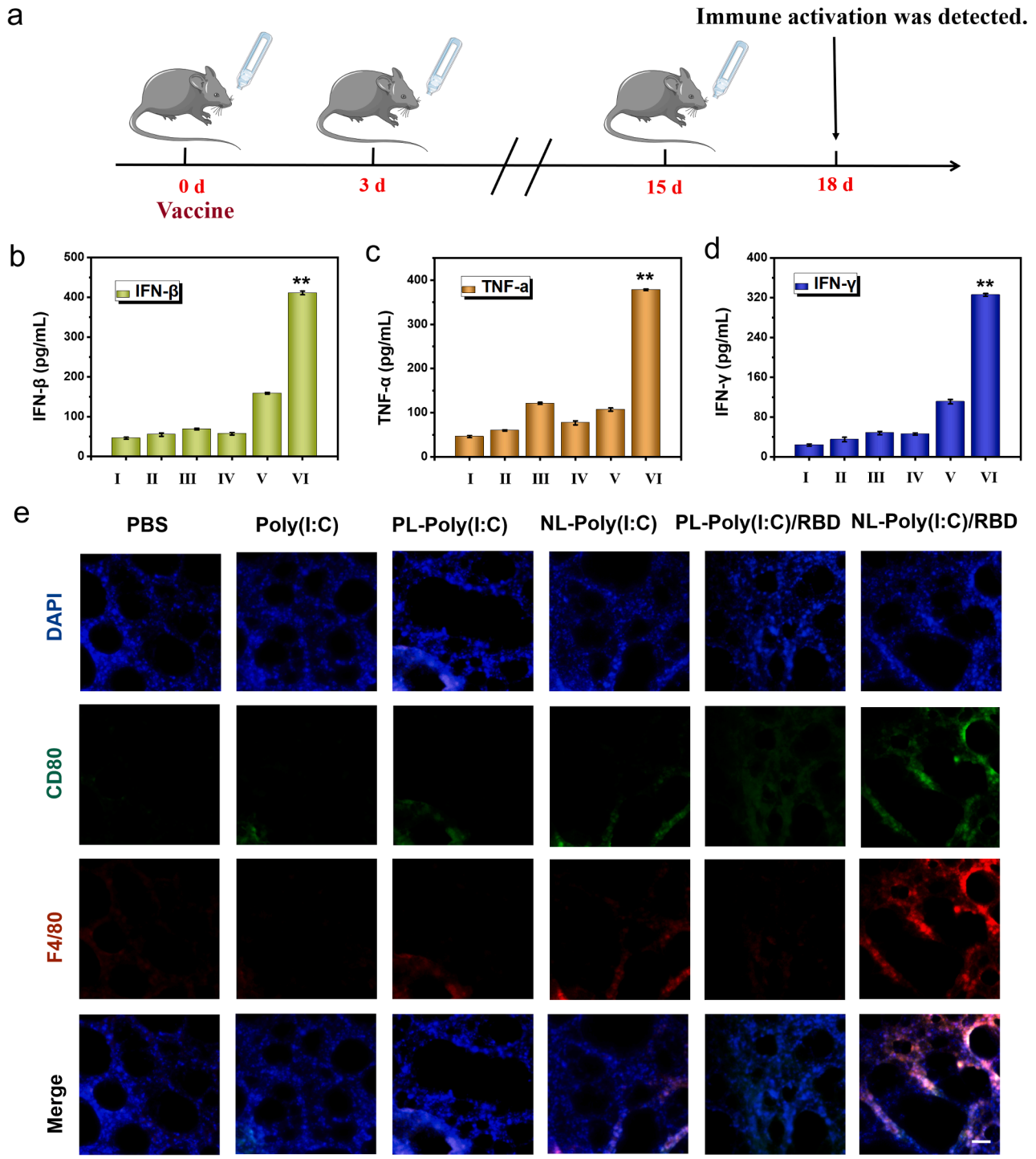

Fig. 3. The immune activation effect of bionic-virus nanovaccine *in vivo*. (a) Experimental flowchart in C57BL/6 mice. (b-d) Secretion levels of IFN-β (b), TNF-α (c) and IFN-γ (d) in BALF. (e) Immunofluorescence staining photographs of lung sections. Scale bars, 100 μm. (I: PBS, II: Poly(I:C), III: PL-Poly(I:C), IV: NL-Poly(I:C), V: PL-Poly(I:C)/RBD, VI: NL-Poly(I:C)/RBD).

interferon receptor.[53] Poly (I:C), a synthetic analog of double-stranded RNA, is a "natural" stimulator of TLR3 signaling pathway. [54] After TLR3 signaling pathway is activated, interferon regulatory factor 3 (IRF3) is phosphorylated by TANK-binding kinase 1 (TBK1), which initiates the expression of interferon in cells (Fig. 2a). Therefore, we used poly (I:C) as an immune activator, packaged in liposomes, which was also completely mimics the RNA genetic material in the coronavirus capsid. After 24 h of different treatments, we examined the activation of TLR3 pathway by western blot (Fig. 2b). In the NL group with PS, the phosphorylated IRF-3 protein band was the most obvious. We also checked the activation of TLR-induced IFN-β in HEK-293 T cells through dual-luciferase reporter assay system (Fig. 2c). Likewise, type I interferon produced the most amount in NL group with PS, indicating that with the help of SP-A and SP-D, the biomimetic virus particles can significantly improve the immune activation efficiency of the TLR3 signaling pathway.

Subsequently, we explored the effect of bionic-virus nanovaccine on macrophage activation *in vitro*. We detected the amount of TNF-α (Fig. 2d). and IL-6 (Fig. 2e) in the supernatant of RAW 264.7 cells after 24 h incubation by ELISA. The results showed that the bionic-virus nanovaccine stimulated macrophages to release cytokines *in vitro*. Especially in the group with PS, the stimulation effect was more obvious, which might be due to the presence of PS that promoted the absorption of NL by RAW 264.7 and enhances their immune activation. The immunofluorescence images of macrophages after 24 h of different treatments could be seen intuitively that, consistent with the ELISA results, the immune stimulation effect of the NL with PS group was the most obvious (Figure S13). Compared with free poly (I:C), the immune stimulation degree of PL group and NL group increased to a certain extent. After adding PS, the activation efficiency of NL group was obviously improved. But for PL group, adding PS had little effect on the activation efficiency. In order to explore whether the bionic-virus nanovaccine can activate immunity in other APC cells, we selected DC 2.4 for *in vitro* cell experiments. As shown in Figure S14 and S15, the NL with PS group activated DCs to produce the largest amount of TNF-α and IL-6. Subsequently, we further checked the activation of macrophages and DCs by flow cytometry. The results of flow cytometry showed that the immune activation of the NL and PS groups was the highest, ten times that of the blank group and seven times that of the no PS group (Fig. 2f, 2 g). Moreover, we also got similar results in DCs (Figure S16).

3.3. Immune excitation of inhalable bionic-virus nanovaccine in Vivo.

Since the immune activation performance of the inhalable bionic-virus nanovaccine had been proven *in vitro*, we speculated that it could also achieve similar immune effect *in vivo*. At the same time, we used free poly (I:C) and positively charged PL as control. The immunization process of bionic-virus nanovaccine in mice was shown in the Fig. 3a. C57BL/6 mice aged 5–6 weeks were intranasally immunized with bionic virus nano vaccine, and the booster immunization was carried out on the third day. The third immunization was performed half a month after the first immunization. For each immunotherapy, 50 μl of the nanovaccine was inhaled via the nasal route. On the third day after the end of immunization, we collected the mouse's trachea, lung and BALF to check the mouse's respiratory tract immune activation. In antiviral immunity, IFN played a vital role, especially type I IFN could protect the body well and prevent viral infection. Therefore, we tested the IFN-β content in BALF, consistent with the experimental results *in vitro*, the group produced the most IFN-β, which meant that NL-RBD had the best protection performance (Fig. 3b). We detected the expression of cytokines including TNF-α and IFN-γ in BALF to further explore the degree of immune activation by ELISA. The increase in cytokines value reflected the activation of AMs (Fig. 3c, 3d). Immunofluorescence staining of lung sections showed that the expression levels of macrophage marker CD80 and F4/80 of RBD protein conjugated NL group were significantly increased (Fig. 3e).

Next, we used flow cytometry to detect APCs activation in various parts of mice. F4/80 is a mature mouse macrophage marker. As shown in Fig. 4a and 4b, the amount of $F4/80^+$ AMs in BALF activated by NL-RBD was 17 times that of free poly (I:C), was 2.3 times that of PL-RBD. The immune activation effect of AMs in the group lacking RBD protein was not obvious. Free poly (I:C) did not produce a strong immune stimulation effect in lung macrophages, which may be due to the instability of poly(I:C) as a double-stranded RNA analog *in vivo*. Compared with NL group, the PL group was less absorbed by AMs, so its immune activation was relatively weak. The group without RBD protein conjugate, because of the lack of antigen protein, the immune activation effect was also limited. For tracheal epithelial cells, the activation of $F4/80^+$ AMs in NL-RBD group was also the most obvious (Figure S17). The differentiation of macrophages in mediastinal lymph nodes (MLNs) also showed the analogous trend (Figure S18). Next, we tested the activation of DCs in MLNs. The $CD86^+$ DCs in the NL-RBD group were nearly seven times higher than that of the control group (Figure S19), and the $CD11c^+$ DCs were more than three times that of the control group (Fig. 4c, 4d). The activation of mature DC marker CD86 and DC marker CD11c indicated that the antigen presentation of DCs was enhanced. DCs also had a weak activation effect in BLAF (Figure S20 and S21). In tracheal epithelial cells, the activation of DCs was more significant (Figure S22 and S23).

$CD4^+$ T is mainly expressed by helper T (Th) cells and was the receptor for Th cell TCR to recognize antigens. It bound to the non-polypeptide region of MHC II molecules and participates in Th cell TCR recognition of antigens process.[55] The increase of $CD4^+$ T cells in BALF in the NL-RBD group proves that the occurrence of antigen presentation and further helped B cells to produce antibodies (Fig. 4e, 4f). For tracheal epithelial cells, $CD4^+$ T cells were also activated in the NL-RBD group (Figure S24). At the same time, the activation of $CD8^+$ T cells in BALF was examined (Figure S25 and S26). $CD8^+$ T cells also called cytotoxic T cells, have the function of killing target cells infected with a virus.[56] $CD8^+$ T cells activated by NL-RBD were also significantly higher than other groups, indicating that the system for killing antigens has been excitated. In order to detect T cells RBD antigens specific, we isolated spleen cells from immunized mice for cell proliferation test (Figure S27). MTT results showed that compared with the control group, the addition of RBD protein caused obvious cell proliferation. Next, we analyzed the splenocytes treated with different methods by flow cytometry (Figure S28). The proportion of $CD4^+$ T and $CD8^+$ T cells increased significantly after RBD stimulation (Figure S29 and S30). These results indicated that the body has induced the specific immune response to RBD antigen of SARS-CoV-2 after the treatment of inhalable bionic virus nanovaccine, but has no adaptive immune response to other components of the vaccine.

Antibodies are that B lymphocytes transform into plasma cells under the stimulation of antigens, and produce antibodies that can specifically bind to the corresponding antigens. Therefore, the activation of B cells is essential for the production of antibodies to neutralize the incoming virus. We detected the B cells makers CD138 and CD45 in the mouse spleen by flow cytometry (Fig. 4g and Figure S31). The amount of $CD138^+$ B cells increased slightly in the PL-RBD group, but increased more in the NL-RBD group. NL-RBD group was more easily absorbed by AMs, so the NL-RBD group had stronger immune activation. $CD138^+$ B cells were also weakly activated in the BALF (Figure S32). NL-RBD also activated central memory T cells (Tcm) in BALF (Figure S33). CD62L and CD44 as markers of Tcm stained with PE anti-CD62L and APC anti-CD44, respectively. Then, we detected the immunoglobin G (IgG) titer in the blood of mice (Fig. 4h). Consistent with the results of $CD138^+$ B cells activation, the titer of IgG in the blood of the NL-RBD group was highest. These results proved that the experimental group had the strongest immune activation effect. Due to the unique way of nasal delivery of bionic-virus nanovaccine, it can stimulate the body's strong mucosal immunity and activate high titer sIgA in BALF (Fig. 4i). The function of antibody was evaluated by pseudovirus neutralization test (Fig. 4j). Compared with other groups, NL-RBD group serum could effectively

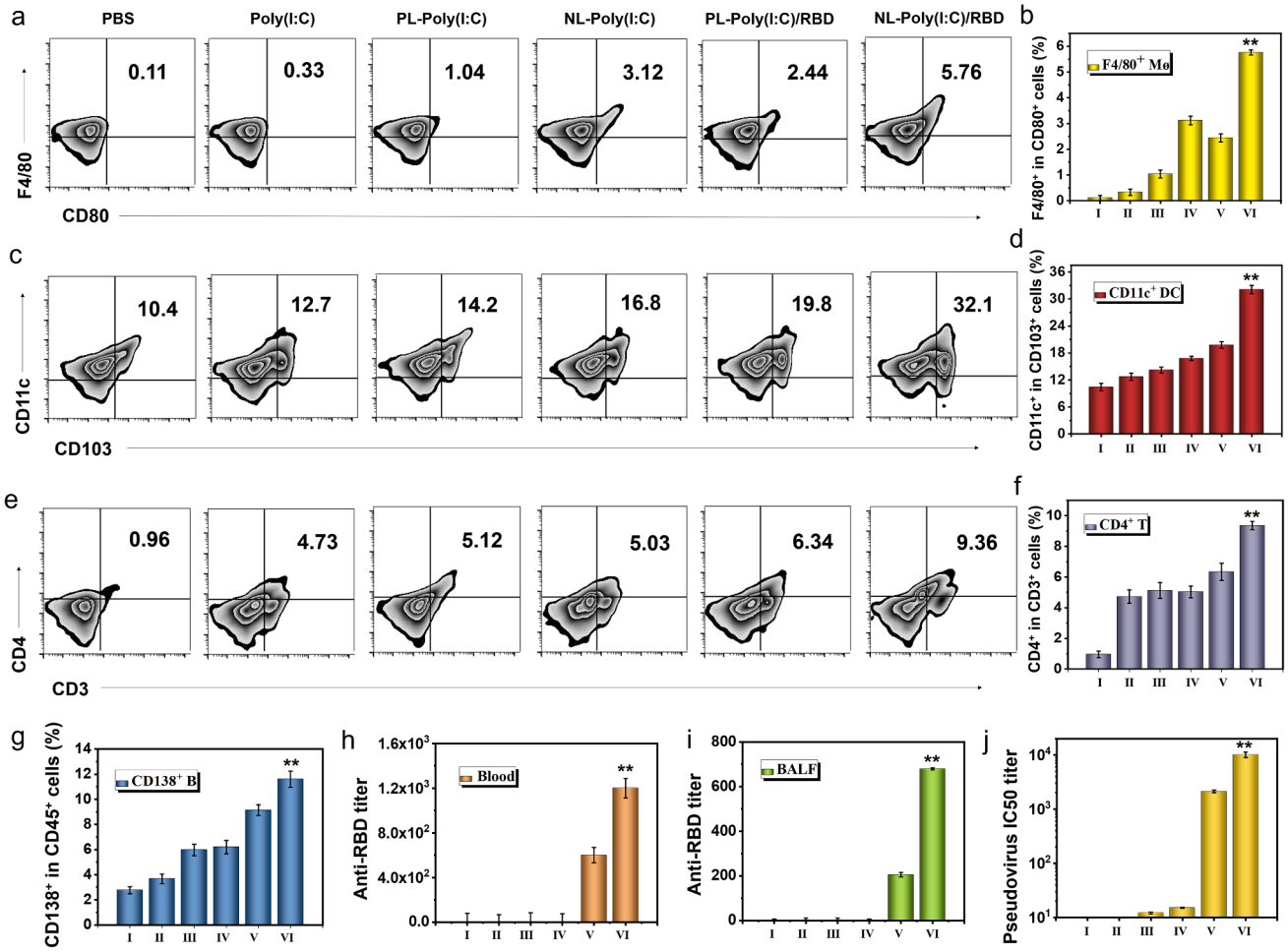

Fig. 4. APC activation and antibody production after bionic-virus nanovaccine *in vivo*. (a) Representative flow cytometry analysis images of F4/80$^+$CD80$^+$ cells in BALF. (b) Relative quantification of F4/80$^+$CD80$^+$ cells in BALF. (c) Representative flow cytometric analysis images of CD11c$^+$CD103$^+$ DCs in mediastinal lymph nodes (MLNs). (d) Relative quantification of CD11c$^+$CD103$^+$ DCs in MLNs. (e) Representative flow cytometric analysis images of CD4$^+$CD3$^+$ T cells in BALF. (f) Relative quantification of CD4$^+$CD3$^+$ T cells in BALF. (g) Relative quantification of CD138$^+$CD45$^+$ B cells in spleens. (h) Anti-RBD IgG titer. (i) Anti-RBD sIgA titer. (j) PsV IC_{50} inhibition titer of serum. (I: PBS, II: Poly(I:C), III: PL-Poly(I:C), IV: NL-Poly(I:C), V: PL-Poly(I:C)/RBD, VI: NL-Poly(I:C)/RBD).

inhibit virus entry. These results suggested that NL-RBD could excite mucosal immune system of respiratory and produced large amounts of sIgA, which could neutralize pathogens. Since the main transmission route of SARS-CoV-2 was respiratory droplets, the activation of mucosal immunity and the production of sIgA might be more effective in protecting the body.

Next, we verified the safety of the vaccine *in vivo*. After vaccination, the blood creatinine value remained in the normal range, indicating that the kidney functions of the mice were not impaired (Figure S34). The morphology of the blood cells of the mice in each group also remained normal (Figure S35). The H&E section showed that there was no inflammation in the mouse heart, liver, spleen, lung and kidney, indicating that the vaccine has excellent biocompatibility (Figure S36).

3.4. *The protection of inhalable bionic-virus nanovaccine against virus attack.*

In order to verify the protective effect of the vaccine after the virus challenge, we transfected hACE2 plasmid with cationic reagents into the mouse respiratory tract by nasal administration to form SARS-CoV-2 susceptible mice on the fifth day after three immunizations. Transfection of hACE2 plasmid once a day for two consecutive days. On the third day after plasmid transfection, mice were challenged with pseudovirus by nasal delivery, which was a replication-defective virus based on the HIV lentivirus packaging system based on the spike protein of SARS-CoV-2 as the pseudovirus spike protein, and had no pathogenic ability. And on the third day after pseudovirus challenge, the mice were dissected and analyzed (Fig. 5a). Compared with the control group, the secretion of TNF-α (Fig. 5b) and IFN-γ (Fig. 5c) in BALF of NL-RBD group was significantly increased after the mice were challenged with pseudovirus, indicating that the immune system was activated. And in wild-type (WT) mice, the secretion of cytokines was slightly lower than that of modified mice, but there was a similar trend among the groups. Type I INF is essential for inhibiting virus replication and modulating the antiviral immune response, so we detected the amount of INF-β (Fig. 5d) in BALF by ELISA. INF-β is produced most in the NL-RBD group. In other words, the NL-RBD group had a stronger ability to resist SARS-CoV-2 and prevent virus invasion.

Since AMs in the lungs are activated first, we checked the activation of AMs in BALF of each group of mice by flow cytometry (Fig. 5e, 5f). Both of WT mice and hACE2 mice, the activation of AMs was the most obvious in the NL-RBD group after virus challenge, and there was little difference in activation degree of two type mice. A possible explanation for this might be that whether the mice were susceptible to SARS-CoV-2, AMs had similar immune effects to antigens. Macrophages in tracheal epithelial cells also weakly differentiate (Figure S37). The following, we checked the immune activation in the MLNs of the mice. The activation of CD86$^+$ DCs (Fig. 5g and S38) in the NL-RBD group was more than

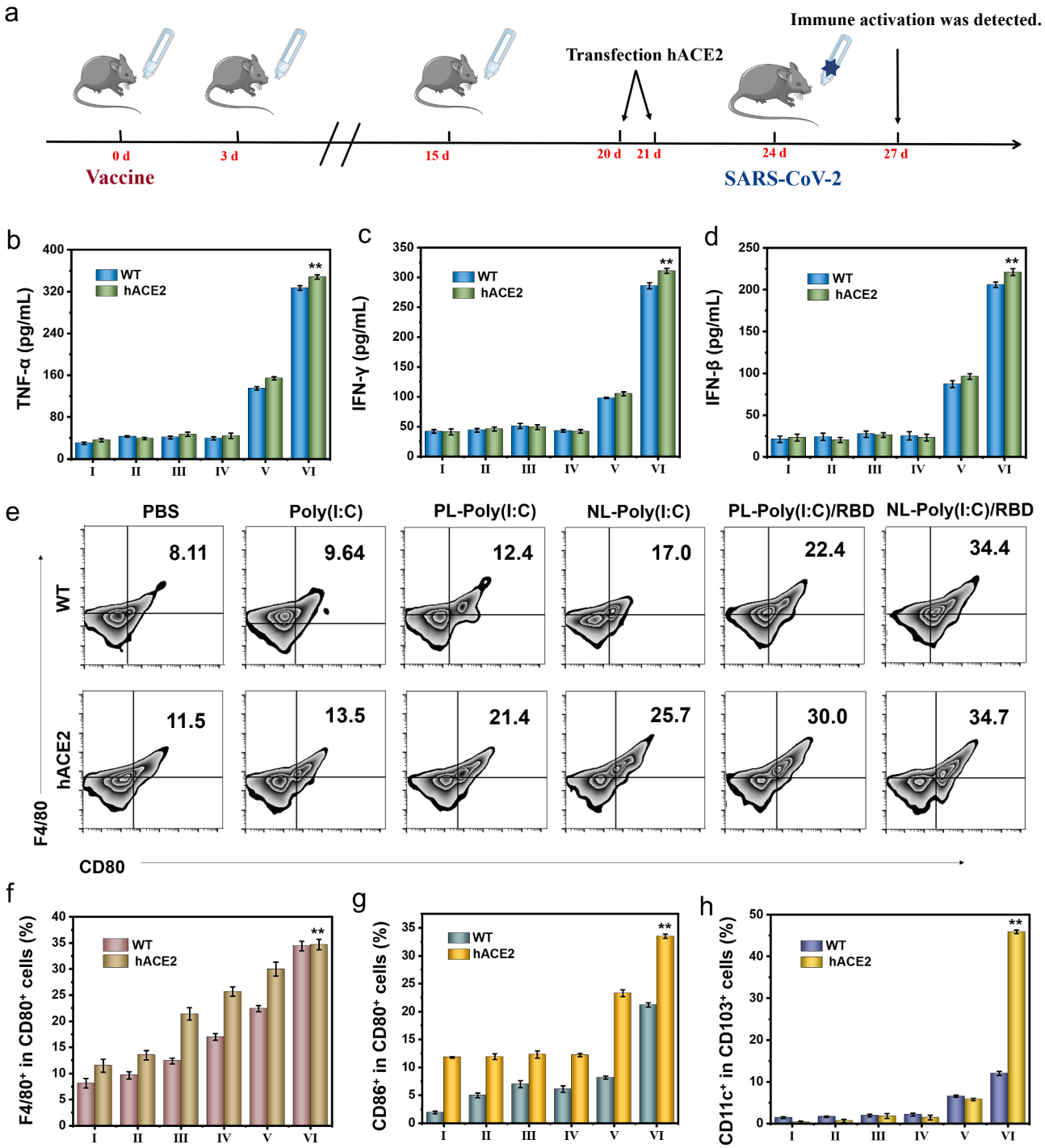

Fig. 5. The immune activation function after pseudovirus challenge in WT mice and hACE2 mice models. (a) Experimental flowchart in C57BL/6 mice. (b-d) Secretion levels of TNF-α (b), IFN-γ (c) and IFN-β (d) in BALF of WT mice and hACE2 mice. (e) Representative flow cytometric analysis images of F4/80$^+$CD80$^+$ AMs in BALF of WT mice and hACE2 mice. (f) Relative quantification of F4/80$^+$CD80$^+$ AMs in BALF of WT mice and hACE2 mice. (g) Relative quantification of CD86$^+$CD80$^+$ DCs in MLNs of WT mice and hACE2 mice. (h) Relative quantification of CD11c$^+$CD103$^+$ DCs in MLNs of WT mice and hACE2 mice. (I: PBS, II: Poly(I:C), III: PL-Poly(I:C), IV: NL-Poly(I:C), V: PL-Poly(I:C)/RBD, VI: NL-Poly(I:C)/RBD).

three times that of the control group, and the activation of CD11c$^+$ DCs (Fig. 5h and S39) was dozens of times that of the control group. The activation of lymph node macrophages also showed the same trend, F4/80$^+$ cells in the NL-RBD group are 60 times that of the control group in hACE2 mice (Figure S40). And compared with WT mice, the activation trend of APC cells in the MLNs of hACE2 mice was more obvious. This might be due to the susceptibility of hACE2 mice making the virus easier to recognize by cells, exciting the process of antigen presentation, leading to stronger immune stimulation.

Mature T cells are distributed through the bloodstream to settle in the thymus-dependent areas of peripheral immune organs, and could be recirculated through lymphatic vessels, peripheral blood and tissue fluid, etc., to exert immune regulation functions. We further tested the effect of NL-RBD on cellular immunity in two kinds of mice. CD4$^+$ T cells were partially activated in the PL-RBD group in hACE2 mice, and the CD4$^+$ T cells in the NL-RBD group had the highest degree of activation

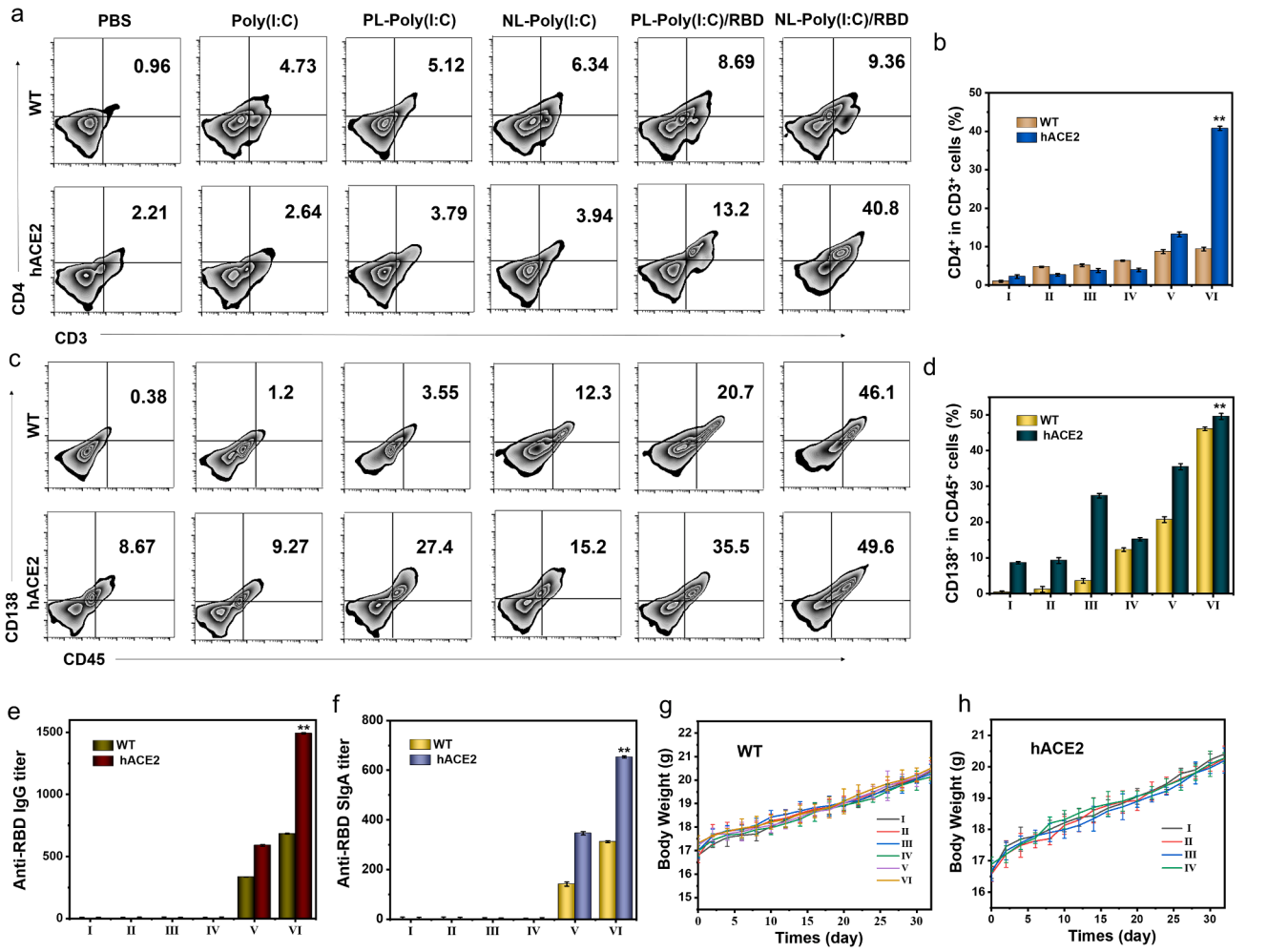

Fig. 6. Initiation of immune memory after pseudovirus challenge in WT mice and hACE2 mouse models. (a) Representative flow cytometric analysis images of $CD4^+CD3^+$ T cells in BALF of WT mice and hACE2 mice. (b) Relative quantification of $CD4^+CD3^+$ T cells in BALF of WT mice and hACE2 mice. (c) Representative flow cytometric analysis images of $CD138^+CD45^+$ B cells in spleen of WT mice and hACE2 mice. (d) Relative quantification of $CD138^+CD45^+$ B cells in spleen of WT mice and hACE2 mice. (e) Anti-RBD IgG titer in blood of WT mice and hACE2 mice. (f) Anti-RBD sIgA titer in BALF of WT mice and hACE2 mice. (g,h) Body weight of WT (g) and hACE2 (h) mice during the one month evaluation period. (I: PBS, II: Poly(I:C), III: PL-Poly(I:C), IV: NL-Poly(I:C), V: PL-Poly(I:C)/RBD, VI: NL-Poly(I:C)/RBD).

(Fig. 6a, 6b). And it could be noticed that the proportion of $CD4^+$ T cells in the WT group was significantly lower than that in the hACE2 group. In addition, the activation of $CD8^+$ T cells was similar (Figure S41). Although the NL-RBD group in WT mice could also activate $CD8^+$ T cells, the activation efficiency was much lower than that in hACE2 mice. Then, we checked the central memory T cell (Tcm) differentiation in MLNs (Figure S42). Tcm is a T lymphocyte with long-term memory produced by naive T Cell after antigen activation, and home to lymph nodes to receive antigen re-stimulation. Even if only a small number of memory T cells can rapidly differentiate into effector T cells under the action of a small number of antigen stimulation or costimulatory molecular signals, so as to effectively eliminate the invading virus. Therefore, Tcm plays a crucial role in the immune memory of cellular immunity. NL-RBD caused the activation of Tcm cells in both WT mice and hACE2 mice, but the activation effect was stronger in hACE2 mice. This proved that NL-RBD could very well stimulate the immune memory effect in susceptible mice.

Following, we checked the humoral immune activation in each group of mice by flow cytometry and ELISA. B lymphocytes could differentiate into plasma cells under antigen stimulation, and plasma cells could synthesize and secrete antibodies, which mainly performed the body's humoral immunity. As shown in Fig. 6c and 6d, the proportion of $CD138^+$ B cells in spleen of NL-RBD group increased significantly in both WT and hACE2 mice. In hACE2 mice tracheal epithelial cells, B cells also differentiated significantly, with the same differentiation trend as in the spleen (Figure S43). Increased proportion of $CD138^+$ B cell results demonstrated that humoral immunity was activated. Then, we detected the secretion of IgG in mouse blood (Fig. 6e) and sIgA in BALF (Fig. 6f). NL-RBD treatment induced high titers of IgG and SIgA against RBD. These results suggested that the vaccine has the potential to protect mice from virus infection. The body weights of WT and hACE2 mice after pseudovirus challenge (mice challenged with pseudovirus on day 0) were kept within a stable range (Fig. 6g and 6 h). And at the same time, the blood creatinine value of hACE2 mice was checked (Figure S44). The creatinine values of the mice in each group of mice remained at a normal level and did not cause infection, further indicating the safety of the vaccine.

3.5. Immune activation by different administration routes of bionic-virus nanovaccine.

Notably, SARS-CoV-2 is mainly transmitted through the respiratory tract, so we speculate that the activation of mucosal immunity can effectively prevent the infection and spread of SARS-CoV-2. We compared the differences in immune activation and body protection of several different administration routes (Fig. 7a). We used the methods of

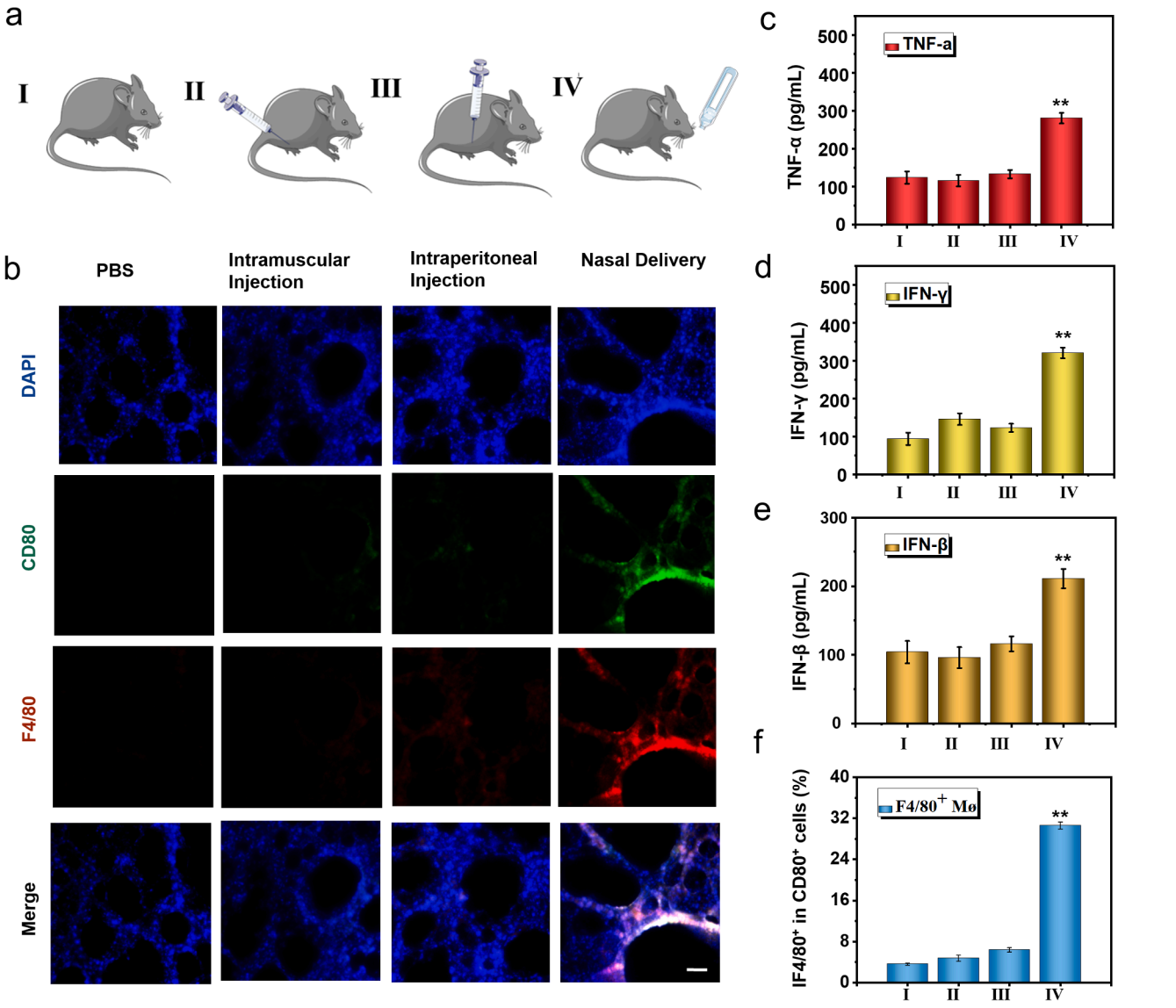

Fig. 7. Influence of different administration routes on the immune effect of bionic-virus nanovaccine. (a) Schematic diagram of grouping mice with different administration methods. (b) Immunofluorescence staining of lung sections. Scale bars, 100 μm. (c-e) Secretion levels of TNF-α (c), IFN-γ (d) and IFN-β (e) in BALF. (f) Relative quantification of F4/80$^+$CD80$^+$ AMs in BALF. (I: PBS, II: Intramuscular Injection, III: Intraperitoneal Injection, IV: Nasal Delivery).

intramuscular injection (50 μl NL-RBD), intraperitoneal injection (50 μl NL-RBD) and nasal delivery (50 μl NL-RBD) to immunize hACE2 mice three times. In the PBS group, the same volume of PBS was dripped into the nasal cavity. The first immunization was three days apart from the second, and the third immunization was performed half a month after the first immunization. Three days after the end of the immunization, lungs of each group mice were collected and performed section immunostaining (Fig. 7b). Only the nasal delivery group had the strongest expression of CD80$^+$ and F4/80$^+$, and the intramuscular injection and intraperitoneal injection group had little change compared with the control group. And one week after the end of the immunization, we used pseudovirus of SARS-CoV-2 to challenge the mice and checked the results of immune activation in the mice. We detected the secretion of cytokines in BALF by ELISA, the nasal delivery group had the strongest activation of TNF-α (Fig. 7c) and IFN-γ (Fig. 7d). For IFN-β, which had the significant antiviral effect, was the highest in the nasal delivery group (Fig. 7e). Next, we checked the differentiation of macrophages in BALF (Fig. 7f and S45). The activation of macrophages in the nasal delivery group was nearly five times that of the intramuscular injection and intraperitoneal injection groups, that showed nasal delivery activated the respiratory immune system well.

Then, we checked the activation of CD86$^+$ DCs (Figure S46) and CD11c$^+$ DCs (Figure S47) in the tracheal epithelial cells. The activation of DCs in the tracheal epithelial cells in the intramuscular injection and intraperitoneal injection groups was weak. The activation of DCs in BALF showed the same trend, the nasal delivery group had the highest proportion of CD103$^+$CD11c$^+$ DCs (Figure S48). Nasal delivery could well activate DCs and stimulate respiratory mucosal immunity. Nasal delivery could also stimulate the differentiation of CD4$^+$ T cells in the BALF (Fig. 8a, 8b) and tracheal epithelial cells (Figure S49). The increased activation of CD4$^+$ T cells could promote humoral immune activation, which was beneficial to the production of neutralizing antibodies. Afterward, we checked the differentiation of Tcm in BALF (Fig. 8c). As shown in Fig. 8d, the activation efficiency of nasal delivery group is more than ten times that of the other two immune routes. The differentiation trend of Tcm cells in tracheal epithelial was the same as that in BALF (Figure S50), nasal delivery could well activate respiratory mucosal immunity and form immune memory. At the same time, we checked the activation of B cells in the spleen (Fig. 8e, 8f), and the activation efficiency of the nasal delivery group was significantly higher

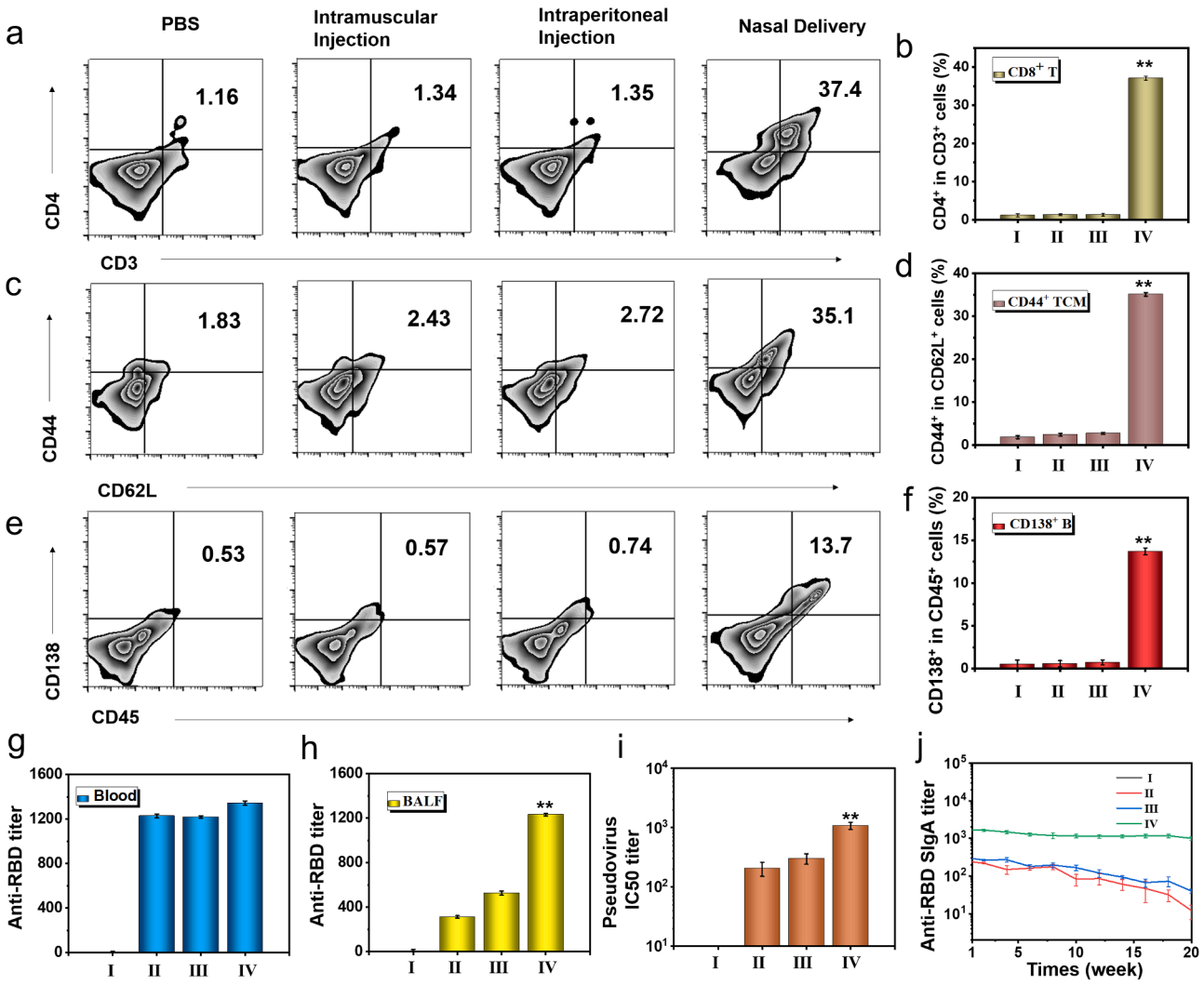

Fig. 8. Immune protection of different administration routes of bionic-virus nanovaccine. (a) Representative flow cytometric analysis images of $CD4^+CD3^+$ T cells in BALF. (b) Relative quantification of $CD4^+CD3^+$ T cells in BALF. (c) Representative flow cytometric analysis images of $CD44^+CD62L^+$ TCM cells in BALF. (d) Relative quantification of $CD44^+CD62L^+$ TCM cells in BALF. (e) Representative flow cytometric analysis images of $CD138^+CD45^+$ B cells in spleen. (f) Relative quantification of $CD138^+CD45^+$ B cells in spleen. (g) Anti-RBD IgG titer. (h) Anti-RBD sIgA titer. (i) PsV IC_{50} inhibition titer of BALF. (j) Anti-RBD sIgA titer of mice during the five months evaluation period. (I: PBS, II: Intramuscular Injection, III: Intraperitoneal Injection, IV: Nasal Delivery).

than that of the other groups, indicating that the vaccines could effectively induce humoral immunity.

Finally, the protective effects of different inoculation methods were discussed. The IgG titer in the blood of the nasal delivery group was similar to the intramuscular injection and intraperitoneal injection groups (Fig. 8g). However, the sIgA titer in the BALF of the nasal delivery group was hundreds of times of the intramuscular injection and intraperitoneal injection groups (Fig. 8h). Under pseudovirus challenge, nasal delivery could activate mucosal immunity more quickly to produce more sIgA to protect the body. The results of the pseudovirus neutralization experiment proved that BALF of the nasal administration group has the best effect in inhibiting pseudovirus infection, showcasing its potential in the prevention of SARS-CoV-2 (Fig. 8i). In addition, compared with other groups, the sIgA protection time of nasal delivery group was the longest, lasting at least five months (Fig. 8j). The blood creatinine value of each group of mice was in the normal range (Figure S51). And the body weight change curve of mice (the mice were challenged with pseudovirus on day 0) showed that the body weight of each group of mice was at normal level (Figure S52). The results of H&E staining of main organs also showed that there was no inflammation (Figure S53). Taken together, these results suggested that the safety of the inhalable bionic-virus nanovaccine used *in vivo*.

4. Conclusion

This study was undertaken to design an inhalable bionic-virus nanovaccine for nasal delivery to induce mucosal immunity response and improve the effectiveness of the COVID-2019 vaccine. Since the main route of SARS-CoV-2 transmission is respiratory droplets, the excitation of respiratory mucosal immunity is vitally important for the prevention of virus. The inhalable nanovaccine has a structure similar to that of SARS-CoV-2, including nucleic acid (Ploy I:C), capsid (biomimetic PS layer liposomes), and spike protein (RBD), and is administered through nasal delivery to simulate the virus infection process. Poly (I:C) can trigger the secretion of a variety of immune-activated cytokines by stimulating TLR signaling pathway, and further help RBD to mature DCs, helper T cells and B cells. Compared with the hACE2 mice vaccinated intramuscularly and intraperitoneally, mice administered nasally inspired better mucosal immunity response capacity and produced high titer sIgA against SARS-CoV-2 in the respiratory mucosal. The results of virus challenge experiment indicated that the inhalable nanovaccine strategy could play an excellent protective effect in the body. Although

we have achieved a pleasing effect, further studies need to be carried out in order to validate the preventive effect of inhalable bionic-virus nanovaccine against wild type SARS-CoV-2 infection in non-human primate for closer to the process of human infection with the virus before the clinical trial. According to our preliminary results, in contrast to traditional injectable vaccines, the inhalable nanovaccine can better inspire respiratory mucosal immunity and secrete large amounts of sIgA on the mucosal surface as a barrier against virus invasion, as well as avoid pain and potential infection. Hence, the strategy of nasal immunization with inhalable bionic-virus nanovaccine strategy that may possess wider application potential for respiratory infectious disease against many emerging pandemics.

Ethical Statement

All the animal experiments involved in this work were approved by the Animal Ethics Committee of Tianjin University.

Declaration of Competing Interest

The authors declare that they have no known competing financial interests or personal relationships that could have appeared to influence the work reported in this paper.

Acknowledgement

This work supported by the National Natural Science Foundation of China (32000999, 81925020 and 81630051), the Key Project of Tianjin Natural Science Foundation (19JCZDJC34100) and the National Key R&D Program of China (2017YFB1300302).

Appendix A. Supplementary data

Supplementary data to this article can be found online at https://doi.org/10.1016/j.cej.2021.129392.

References

[1] J.-M. Pawlotsky, COVID-19 and the liver-related deaths to come, Nature Reviews, Gastroenterology & Hepatology 17 (2020) 523–525.
[2] J. Cohen, D. Normile, New SARS-like virus in China triggers alarm, Science 367 (2020) 234–235.
[3] L. Corey, J.R. Mascola, A.S. Fauci, F.S. Collins, A strategic approach to COVID-19 vaccine R&D, Science 368 (2020) 948–950.
[4] Q. Gao, L. Bao, H. Mao, L. Wang, K. Xu, M. Yang, Y. Li, L. Zhu, N. Wang, Z. Lv, H. Gao, X. Ge, B. Kan, Y. Hu, J. Liu, F. Cai, D. Jiang, Y. Yin, C. Qin, J. Li, X. Gong, X. Lou, W. Shi, D. Wu, H. Zhang, L. Zhu, W. Deng, Y. Li, J. Lu, C. Li, X. Wang, W. Yin, Y. Zhang, C. Qin, Development of an inactivated vaccine candidate for SARS-CoV-2, Science 369 (2020) 77-+.
[5] M. Jeyanathan, S. Afkhami, F. Smaill, M.S. Miller, B.D. Lichty, Z. Xing, Immunological considerations for COVID-19 vaccine strategies, Nature Reviews Immunology 20 (2020) 615–632.
[6] J.R. Schaefer Y. Sharkova T. Nickolaus A SARS-CoV-2 mRNA Vaccine - Preliminary Report The New England journal of medicine 383 2020 1191 1191.
[7] T. Thanh Le, Z. Andreadakis, A. Kumar, R. Gomez Roman, S. Tollefsen, M. Saville, S. Mayhew, The COVID-19 vaccine development landscape, Nature Reviews Drug Discovery 19 (2020) 305–306.
[8] F. Wang, R.M. Kream, G.B. Stefano, An Evidence Based Perspective on mRNA-SARS-CoV-2 Vaccine Development, Medical Science Monitor 26 (2020).
[9] J. Yu, L.H. Tostanoski, L. Peter, N.B. Mercado, K. McMahan, S.H. Mahrokhian, J. P. Nkolola, J. Liu, Z. Li, A. Chandrashekar, D.R. Martinez, C. Loos, C. Atyeo, S. Fischinger, J.S. Burke, M.D. Slein, Y. Chen, A. Zuiani, F.J.N. Lelis, M. Travers, S. Habibi, L. Pessaint, A. Van Ry, K. Blade, R. Brown, A. Cook, B. Finneyfrock, A. Dodson, E. Teow, J. Velasco, R. Zahn, F. Wegmann, E.A. Bondzie, G. Dagotto, M. S. Gebre, X. He, C. Jacob-Dolan, M. Kirilova, N. Kordana, Z. Lin, L.F. Maxfield, F. Nampanya, R. Nityanandam, J.D. Ventura, H. Wan, Y. Cai, B. Chen, A. G. Schmidt, D.R. Wesemann, R.S. Baric, G. Alter, H. Andersen, M.G. Lewis, D. H. Barouch, DNA vaccine protection against SARS-CoV-2 in rhesus macaques, Science 369 (2020) 806-+.
[10] N.-N. Zhang, X.-F. Li, Y.-Q. Deng, H. Zhao, Y.-J. Huang, G. Yang, W.-J. Huang, P. Gao, C. Zhou, R.-R. Zhang, Y. Guo, S.-H. Sun, H. Fan, S.-L. Zu, Q. Chen, Q. He, T.-S. Cao, X.-Y. Huang, H.-Y. Qiu, J.-H. Nie, Y. Jiang, H.-Y. Yan, Q. Ye, X. Zhong, X.-L. Xue, Z.-Y. Zha, D. Zhou, X. Yang, Y.-C. Wang, B. Ying, C.-F. Qin, A Thermostable mRNA Vaccine against COVID-19, Cell 182 (2020) 1271-+.
[11] F.-C. Zhu, Y.-H. Li, X.-H. Guan, L.-H. Hou, W.-J. Wang, J.-X. Li, S.-P. Wu, B.-S. Wang, Z. Wang, L. Wang, S.-Y. Jia, H.-D. Jiang, L. Wang, T. Jiang, Y. Hu, J.-B. Gou, S.-B. Xu, J.-J. Xu, X.-W. Wang, W. Wang, W. Chen, Safety, tolerability, and immunogenicity of a recombinant adenovirus type-5 vectored COVID-19 vaccine: a dose-escalation, open-label, non-randomised, first-in-human trial, The Lancet 395 (2020) 1845–1854.
[12] F. Krammer, SARS-CoV-2 vaccines in development, Nature (2020).
[13] S.E. Oliver, J.W. Gargano, M. Marin, M. Wallace, K.G. Curran, M. Chamberland, N. McClung, D. Campos-Outcalt, R.L. Morgan, S. Mbaeyi, J.R. Romero, H.K. Talbot, G. M. Lee, B.P. Bell, K. Dooling, The Advisory Committee on Immunization Practices' Interim Recommendation for Use of Pfizer-BioNTech COVID-19 Vaccine - United States, December 2020, MMWR. Morbidity and mortality weekly report 69 (2020) 1922-1924.
[14] H. Ledford, Moderna COVID vaccine becomes second to get US authorization, Nature (2020).
[15] C.Q. Ma, S. Su, J.C. Wang, L. Wei, L.Y. Du, S.B. Jiang, From SARS-CoV to SARS-CoV-2: safety and broad-spectrum are important for coronavirus vaccine development, Microbes and Infection 22 (2020) 245–253.
[16] D. Hobernik, M. Bros, DNA VaccinesHow Far From Clinical Use? Int. J. Mol. Sci. 19 (2018) 28.
[17] W.W. Leitner, H. Ying, N.P. Restifo, DNA and RNA-based vaccines: principles, progress and prospects, Vaccine 18 (1999) 765–777.
[18] T. Kramps, J. Probst, Messenger RNA-based vaccines: progress, challenges, applications, Wiley Interdiscip, Rev.-RNA 4 (2013) 737–749.
[19] N.A.C. Jackson, K.E. Kester, D. Casimiro, S. Gurunathan, F. DeRosa, The promise of mRNA vaccines: a biotech and industrial perspective, npj Vaccines 5 (2020) 6.
[20] T.T. Le, J.P. Cramer, R. Chen, S. Mayhew, Evolution of the COVID-19 vaccine development landscape, Nature reviews. Drug discovery 19 (2020) 667–668.
[21] T. Acter, N. Uddin, J. Das, A. Akhter, T.R. Choudhury, S. Kim, Evolution of severe acute respiratory syndrome coronavirus 2 (SARS-CoV-2) as coronavirus disease 2019 (COVID-19) pandemic: A global health emergency, Sci. Total Environ. 730 (2020) 19.
[22] B. Rockx, T. Kuiken, S. Herfst, T. Bestebroer, M.M. Lamers, B.B.O. Munnink, D. de Meulder, G. van Amerongen, J. van den Brand, N.M.A. Okba, D. Schipper, P. van Run, L. Leijten, R. Sikkema, E. Verschoor, B. Verstrepen, W. Bogers, J. Langermans, C. Drosten, M.F. van Vlissingen, R. Fouchier, R. de Swart, M. Koopmans, B. L. Haagmans, Comparative pathogenesis of COVID-19, MERS, and SARS in a nonhuman primate model, Science 368 (2020) 1012-+.
[23] L. Boes, B. Boedeker, P. Schmich, M. Wetzstein, O. Wichmann, C. Remschmidt, Factors associated with parental acceptance of seasonal influenza vaccination for their children - A telephone survey in the adult population in Germany, Vaccine 35 (2017) 3789–3796.
[24] K.R. Van Kampen, Z.K. Shi, P. Gao, J.F. Zhang, K.W. Foster, D.T. Chen, D. Marks, C. A. Elmets, D.C.C. Tang, Safety and immunogenicity of adenovirus-vectored nasal and epicutaneous influenza vaccines in humans, Vaccine 23 (2005) 1029–1036.
[25] J. Xu, S. Li, X. Wang, J. Liu, P. Shan, Y. Zhou, J. Zhao, Z. Wang, C. Xu, M. Chen, Z. Chen, K. Zhao, D. Qu, Systemic and mucosal humoral immune responses induced by the JY-adjuvanted nasal spray H7N9 vaccine in mice, Emerging Microbes & Infections 7 (2018).
[26] N.J. Mantis, N. Rol, B. Corthesy, Secretory IgA's complex roles in immunity and mucosal homeostasis in the gut, Mucosal Immunol. 4 (2011) 603–611.
[27] M. Ejemel, Q. Li, S. Hou, Z.A. Schiller, J.A. Tree, A. Wallace, A. Amcheslavsky, N. K. Yilmaz, K.R. Buttigieg, M.J. Elmore, K. Godwin, N. Coombes, J.R. Toomey, R. Schneider, A.S. Ramchetty, B.J. Close, D.-Y. Chen, H.L. Conway, M. Saeed, C. Ganesa, M.W. Carroll, L.A. Cavacini, M.S. Klempner, C.A. Schiffer, Y. Wang, A cross-reactive human IgA monoclonal antibody blocks SARS-CoV-2 spike-ACE2 interaction, Nature Communications 11 (2020).
[28] F.S. Dawood, J.R. Chung, S.S. Kim, R.K. Zimmerman, M.P. Nowalk, M.L. Jackson, L.A. Jackson, A.S. Monto, E.T. Martin, E.A. Belongia, H.Q. McLean, M. Gaglani, K. Dunnigan, A. Foust, W. Sessions, J. DaSilva, S. Le, T. Stark, R.J. Kondor, J. R. Barnes, D.E. Wentworth, L. Brammer, A.M. Fry, M.M. Patel, B. Flannery, Interim Estimates of 2019–20 Seasonal Influenza Vaccine Effectiveness - United States, Mmwr-Morbidity and Mortality Weekly Report 69 (2020) (February 2020) 177–182.
[29] L.A. Grohskopf, L.Z. Sokolow, K.R. Broder, E.B. Walter, A.M. Fry, D.B. Jernigan, Prevention and Control of Seasonal Influenza with Vaccines: Recommendations of the Advisory Committee on Immunization Practices-United States, 2018–19 Influenza Season, MMWR Recomm. Rep. 68 (2019) 1–20.
[30] L. He, W.G. Xu, X.Q. Wang, C.X. Wang, J.X. Ding, X.S. Chen, Polymer micro/nanocarrier-assisted synergistic chemohormonal therapy for prostate cancer, Biomater. Sci. 6 (2018) 1433–1444.
[31] J.X. Wang, W.G. Xu, S.X. Li, H.P. Qiu, Z.B. Li, C.X. Wang, X.Q. Wang, J.X. Ding, Polylactide-Cholesterol Stereocomplex Micelle Encapsulating Chemotherapeutic Agent for Improved Antitumor Efficacy and Safety, J. Biomed. Nanotechnol. 14 (2018) 2102–2113.
[32] J.J. Chen, J.X. Ding, Y. Zhang, C.S. Xiao, X.L. Zhuang, X.S. Chen, Polyion complex micelles with gradient pH-sensitivity for adjustable intracellular drug delivery, Polym. Chem. 6 (2015) 397–405.
[33] H.H. Xiao, L.S. Yan, E.M. Dempsey, W.T. Song, R.G. Qi, W.L. Li, Y.B. Huang, X. B. Jing, D.F. Zhou, J.X. Ding, X.S. Chen, Recent progress in polymer-based platinum drug delivery systems, Progress in Polymer Science 87 (2018) 70–106.
[34] Y. Wang, Z.Y. Jiang, W.G. Xu, Y.A. Yang, X.L. Zhuang, J.X. Ding, X.S. Chen, Chiral Polypeptide Thermogels Induce Controlled Inflammatory Response as Potential Immunoadjuvants, ACS Appl. Mater. Interfaces 11 (2019) 8725–8730.

[35] Y.C. Fan, R. Kuai, Y. Xup, L.J. Ochyl, D.J. Irvine, J.J. Moon, Immunogenic Cell Death Amplified by Co-localized Adjuvant Delivery for Cancer Immunotherapy, Nano Lett. 17 (2017) 7387–7393.
[36] J.J. Chen, J.X. Ding, W.G. Xu, T.M. Sun, H.H. Xiao, X.L. Zhuang, X.S. Chen, Receptor and Microenvironment Dual-Recognizable Nanogel for Targeted Chemotherapy of Highly Metastatic Malignancy, Nano Lett. 17 (2017) 4526–4533.
[37] H. Guo, F. Li, W. Xu, J. Chen, Y. Hou, C. Wang, J. Ding, X. Chen, Mucoadhesive Cationic Polypeptide Nanogel with Enhanced Penetration for Efficient Intravesical Chemotherapy of Bladder Cancer, Advanced Science 5 (2018) 1800004.
[38] Q. Guan, R. Guo, S. Huang, F. Zhang, J. Liu, Z. Wang, X. Yang, X. Shuai, Z. Cao, Mesoporous polydopamine carrying sorafenib and SPIO nanoparticles for MRI-guided ferroptosis cancer therapy, Journal of Controlled Release 320 (2020) 392–403.
[39] J.R. Wu, G.R. Williams, S.W. Niu, F. Gao, R.R. Tang, L.M. Zhu, A Multifunctional Biodegradable Nanocomposite for Cancer Theranostics, Advanced Science 6 (2019) 12.
[40] E. Parra, J. Perez-Gil, Composition, structure and mechanical properties define performance of pulmonary surfactant membranes and films, Chemistry and Physics of Lipids 185 (2015) 153–175.
[41] J. Wang, P. Li, Y. Yu, Y. Fu, H. Jiang, M. Lu, Z. Sun, S. Jiang, L. Lu, M.X. Wu, Pulmonary surfactant-biomimetic nanoparticles potentiate heterosubtypic influenza immunity, Science 367 (2020) 869-+.
[42] M. Yuan, N.C. Wu, X.Y. Zhu, C.C.D. Lee, R.T.Y. So, H.B. Lv, C.K.P. Mok, I.A. Wilson, A highly conserved cryptic epitope in the receptor binding domains of SARS-CoV-2 and SARS-CoV, Science 368 (2020) 630-+.
[43] K. Imamura, N. Imamachi, G. Akizuki, M. Kumakura, A. Kawaguchi, K. Nagata, A. Kato, Y. Kawaguchi, H. Sato, M. Yoneda, C. Kai, T. Yada, Y. Suzuki, T. Yamada, T. Ozawa, K. Kaneki, T. Inoue, M. Kobayashi, T. Kodama, Y. Wada, K. Sekimizu, N. Akimitsu, Long Noncoding RNA NEAT1-Dependent SFPQ Relocation from Promoter Region to Paraspeckle Mediates IL8 Expression upon Immune Stimuli, Mol. Cell 53 (2014) 393–406.
[44] A. Haczku, Protective role of the lung collectins surfactant protein A and surfactant protein D in airway inflammation, Journal of Allergy and Clinical Immunology 122 (2008) 861–879.
[45] C. Mao, R. Near, V. Shibad, X. Zhong, W. Gao, An IgA mimicry of IgG that binds Polymeric Immunoglobulin Receptor for mucosa transcytosis, Antibody therapeutics 3 (2020) 157–162.
[46] D.G. Ahn, H.J. Shin, M.H. Kim, S. Lee, H.S. Kim, J. Myoung, B.T. Kim, S.J. Kim, Current Status of Epidemiology, Diagnosis, Therapeutics, and Vaccines for Novel Coronavirus Disease 2019 (COVID-19), J. Microbiol. Biotechnol. 30 (2020) 313-324.
[47] W. Tai, L. He, X. Zhang, J. Pu, D. Voronin, S. Jiang, Y. Zhou, L. Du, Characterization of the receptor-binding domain (RBD) of novel coronavirus: implication for development of RBD protein as a viral attachment inhibitor and vaccine Cellular & Molecular Immunology 17 2020 2019 613 620.
[48] C.O. Barnes, A.P. West Jr., K.E. Huey-Tubman, M.A.G. Hoffmann, N.G. Sharaf, P. R. Hoffman, N. Koranda, H.B. Gristick, C. Gaebler, F. Muecksch, J.C.C. Lorenzi, S. Finkin, T. Hagglof, A. Hurley, K.G. Millard, Y. Weisblum, F. Schmidt, T. Hatziioannou, P.D. Bieniasz, M. Caskey, D.F. Robbiani, M.C. Nussenzweig, P. J. Bjorkman, Structures of Human Antibodies Bound to SARS-CoV-2 Spike Reveal Common Epitopes and Recurrent Features of Antibodies, Cell 182 (2020) 828-+.
[49] Q. Zhang, P. Bastard, Z. Liu, J. Le Pen, M. Moncada-Velez, J. Chen, M. Ogishi, I.K. D. Sabli, S. Hodeib, C. Korol, J. Rosain, K. Bilguvar, J. Ye, A. Bolze, B. Bigio, R. Yang, A.A. Arias, Q. Zhou, Y. Zhang, F. Onodi, S. Korniotis, L. Karpf, Q. Philippot, M. Chbihi, L. Bonnet-Madin, K. Dorgham, N. Smith, W.M. Schneider, B.S. Razooky, H.-H. Hoffmann, E. Michailidis, L. Moens, J.E. Han, L. Lorenzo, L. Bizien, P. Meade, A.-L. Neehus, A.C. Ugurbil, A. Corneau, G. Kerner, P. Zhang, F. Rapaport, Y. Seeleuthner, J. Manry, C. Masson, Y. Schmitt, A. Schluter, T. Le Voyer, T. Khan, J. Li, J. Fellay, L. Roussel, M. Shahrooei, M.F. Alosaimi, D. Mansouri, H. Al-Saud, F. Al-Mulla, F. Almourfi, S.Z. Al-Muhsen, F. Alsohime, S. Al Turki, R. Hasanato, D. van de Beek, A. Biondi, L.R. Bettini, M. D'Angio, P. Bonfanti, L. Imberti, A. Sottini, S. Paghera, E. Quiros-Roldan, C. Rossi, A.J. Oler, M.F. Tompkins, C. Alba, I. Vandernoot, J.-C. Goffard, G. Smits, I. Migeotte, F. Haerynck, P. Soler-Palacin, A. Martin-Nalda, R. Colobran, P.-E. Morange, S. Keles, F. Colkesen, T. Ozcelik, K.K. Yasar, S. Senoglu, S.N. Karabela, C. R. Gallego, G. Novelli, S. Hraiech, Y. Tandjaoui-Lambiotte, X. Duval, C. Laouenan, A.L. Snow, C.L. Dalgard, J. Milner, D.C. Vinh, T.H. Mogensen, N. Marr, A.N. Spaan, B. Boisson, S. Boisson-Dupuis, J. Bustamante, A. Puel, M. Ciancanelli, I. Meyts, T. Maniatis, V. Soumelis, A. Amara, M. Nussenzweig, A. Garcia-Sastre, F. Krammer, A. Pujol, D. Duffy, R. Lifton, S.-Y. Zhang, G. Gorochov, V. Beziat, E. Jouanguy, V. Sancho-Shimizu, C.M. Rice, L. Abel, L.D. Notarangelo, A. Cobat, H.C. Su, J.-L. Casanova, C.-S. Clinicians, C. Clinicians, C.G. Imagine, C.C.S.G. French, V.C. C. Co, U.M.C.C. Amsterdam, Biobank, C.H.G. Effort, U. Niaid, T.C.I. Group, Inborn errors of type I IFN immunity in patients with life-threatening COVID-19, Science (New York N.Y.) (2020).
[50] H.M. Lazear, J.W. Schoggins, M.S. Diamond, Shared and Distinct Functions of Type I and Type III Interferons, Immunity 50 (2019) 907–923.
[51] J.S. Lee, S. Park, H.W. Jeong, J.Y. Ahn, S.J. Choi, H. Lee, B. Choi, S.K. Nam, M. Sa, J.-S. Kwon, S.J. Jeong, H.K. Lee, S.H. Park, S.-H. Park, J.Y. Choi, S.-H. Kim, I. Jung, E.-C. Shin, Immunophenotyping of COVID-19 and influenza highlights the role of type I interferons in development of severe COVID-19, Science Immunology 5 (2020).
[52] B. Liu, Q. Liu, L. Yang, S.K. Palaniappan, I. Bahar, P.S. Thiagarajan, J.L. Ding, Innate immune memory and homeostasis may be conferred through crosstalk between the TLR3 and TLR7 pathways, Science Signaling 9 (2016).
[53] D.F. Tough, P. Borrow, J. Sprent, Induction of bystander T cell proliferation by viruses and type I interferon in vivo, Science (New York, N.Y.) 272 (1996) 1947–1950.
[54] L. Alexopoulou, A.C. Holt, R. Medzhitov, R.A. Flavell, Recognition of double-stranded RNA and activation of NF-kappa B by Toll-like receptor 3, Nature 413 (2001) 732–738.
[55] E. Aarntzen, I.J.M. De Vries, W.J. Lesterhuis, D. Schuurhuis, J.F.M. Jacobs, K. Bol, G. Schreibelt, R. Mus, J.H.W. De Wilt, J. Haanen, D. Schadendorf, A. Croockewit, W.A.M. Blokx, M.M. Van Rossum, W.W. Kwok, G.J. Adema, C.J.A. Punt, C. G. Figdor, Targeting CD4(+) T-Helper Cells Improves the Induction of Antitumor Responses in Dendritic Cell-Based Vaccination, Cancer Res. 73 (2013) 19–29.
[56] J.M. Schenkel, K.A. Fraser, V. Vezys, D. Masopust, Sensing and alarm function of resident memory CD8(+) T cells, Nat. Immunol. 14 (2013) 509-+.